Journal of
Ceramic Science
and Technology

J. Ceram. Sci. Technol., **17** [3] 225-236 (2026)
DOI: 10.4416/JCST2026-00004
available online at: http://www.ceramic-science.com
© 2026 Göller Verlag

Application of Silicon Nitride Ceramics in Sports Protection: Whiskers Toughening Mechanism and Impact Fracture Behavior

Xiaoqin Xu*

Department of Physical Education, Hunan International Economics University, Hunan Changsha, 410205, China

received March 19, 2026; received in revised form May 29, 2026; accepted June 6, 2026

Abstract

Silicon nitride (Si_3N_4) ceramics have emerged as promising candidates for high-performance sports protection equipment due to their exceptional combination of mechanical properties, including high hardness, excellent wear resistance, and superior fracture toughness. This study systematically investigates the application potential of silicon nitride ceramics in sports protection through comprehensive characterization of whisker-reinforced composites. Silicon carbide (SiC) whiskers were incorporated into the Si_3N_4 matrix at varying concentrations (0 – 30 vol%) to enhance fracture toughness and impact resistance. The materials were fabricated by means of hot isostatic pressing (HIP) at 1 750 °C under 200 MPa nitrogen pressure. Characterization techniques including X-ray diffraction (XRD), scanning electron microscopy (SEM), transmission electron microscopy (TEM), and mechanical testing were employed to evaluate microstructure-property relationships. The results demonstrate that 20 vol% SiC whisker addition achieves optimal toughening, with fracture toughness reaching 12.6 MPa·m$^{1/2}$, which represents a 260 % improvement over monolithic Si_3N_4. The Vickers hardness ranges from 15.5 to 20.7 GPa, while flexural strength varies between 600 – 980 MPa depending on whisker content and orientation. Impact testing reveals energy absorption capacities of 15 – 28 J for optimized compositions, significantly exceeding conventional polymer-based protective materials. The toughening mechanisms, including whisker pull-out, crack deflection, and bridging, were analyzed by means of fracture surface examination. These findings establish silicon nitride-based ceramics as viable next-generation materials for high-impact sports protection applications, offering superior protection-to-weight ratios compared to existing solutions.

Keywords: Silicon nitride, SiC whiskers, fracture toughness, ceramic composites, toughening mechanisms

I. Introduction

The development of advanced protective equipment represents a critical challenge in modern sports engineering, where the demand for lightweight yet high-performance materials continues to escalate. Traditional polymer-based protective gear, while offering adequate protection for low-impact scenarios, often fails to provide sufficient defense against high-velocity impacts encountered in contact sports, cycling, and extreme athletic activities [1]. Furthermore, the degradation of polymer properties under environmental exposure and repeated loading cycles necessitates frequent replacement, raising both economic and sustainability concerns [2]. These limitations have catalyzed extensive research into ceramic materials as potential alternatives for next-generation sports protection systems [3].

Among ceramic materials, silicon nitride (Si_3N_4) has attracted considerable attention due to its unique combination of properties that align closely with sports protection requirements [4]. The covalent bonding between silicon and nitrogen atoms imparts exceptional hardness (15 – 20 GPa) and elastic modulus (280 – 365 GPa), while the ability to form elongated β-Si_3N_4 grains during sintering enables substantial fracture toughness through self-reinforcement mechanisms [5]. Additionally, silicon nitride exhibits excellent thermal stability, chemical inertness, and biocompatibility, making it suitable for prolonged skin contact during athletic activities [6]. The density of silicon nitride ceramics (3.4 g/cm^3) is approximately 40 % lower than alumina and 60 % lower than steel, offering significant weight advantages for wearable protection systems [7].

Despite these attractive properties, monolithic silicon nitride ceramics suffer from inherent brittleness that limits their application in impact-prone environments [8]. The fracture toughness of conventional Si_3N_4 (3 – 5 MPa·m$^{1/2}$) is insufficient to withstand the dynamic loading conditions typical of sports impacts, where localized stresses can exceed the material's critical threshold [9]. To address this limitation, various toughening strategies have been explored, including transformation toughening with zirconia particles, fiber reinforcement, and whisker incorporation [10]. Among these approaches, silicon carbide (SiC) whisker reinforcement has demonstrated particular

* Corresponding author: CANDYXU1981@163.com

promise due to the thermodynamic compatibility between SiC and Si_3N_4, combined with the exceptional mechanical properties of SiC whiskers (tensile strength > 3 GPa, elastic modulus ~ 450 GPa) [11].

The toughening mechanisms in whisker-reinforced ceramic matrix composites involve complex interactions between propagating cracks and the reinforcing phase [12]. When a crack encounters a whisker, several energy dissipation mechanisms may activate: crack deflection around the whisker, whisker bridging across the crack wake, and whisker pull-out from the matrix [3]. The relative contribution of each mechanism depends on factors including whisker aspect ratio, volume fraction, interfacial bonding strength, and matrix microstructure [13]. Understanding and optimizing these parameters is essential for developing silicon nitride composites with enhanced impact resistance suitable for sports protection applications [14].

Previous studies have primarily focused on SiC whisker-reinforced Si_3N_4 for high-temperature structural applications, with limited investigation of their behavior under dynamic impact loading relevant to sports protection [15]. Furthermore, the relationship between whisker orientation, distribution, and impact energy absorption remains inadequately characterized (16). This study addresses these gaps by systematically investigating the microstructure, mechanical properties, and impact fracture behavior of SiC whisker-reinforced silicon nitride ceramics with varying whisker contents. The specific objectives include: (1) fabricating dense Si_3N_4-SiC whisker composites with controlled microstructures; (2) characterizing the effects of whisker content on density, hardness, strength, and fracture toughness; (3) evaluating impact resistance through drop-weight and ballistic testing; (4) analyzing toughening and energy absorption mechanisms through detailed fracture surface examination; and (5) assessing the feasibility of these materials for sports protection applications based on performance metrics and comparative analysis with existing solutions [17].

II. Materials and Methods

(1) Raw materials and powder preparation

The starting materials for composite fabrication included high-purity alpha-Si_3N_4 powder (UBE Industries, SN-E10, purity > 99.9 %, average particle size 0.5 μm, specific surface area 9.5 m^2/g), beta-Si_3N_4 seed crystals (0.5 wt%, average length 2 μm), and beta-SiC whiskers (Tokai Carbon, purity > 99 %, average diameter 0.8 μm, average length 20 μm, aspect ratio approximately 25) [18]. The sintering additives consisted of Y_2O_3 (Shin-Etsu Chemical, purity > 99.9 %, 6 wt%) and Al_2O_3 (Sumitomo Chemical, purity > 99.9 %, 2 wt%), which form a liquid phase during sintering to promote densification [4]. The SiC whiskers used for the treated batches were pre-treated in air at 700 °C for 2 h to form a thin silica-rich surface layer that improves wetting by the Y-Al-Si-O liquid phase during sintering [19]. This treatment is not interpreted as producing a retained, discrete oxide shell after HIP; rather, the surface oxide is expected to participate in the interfacial silicate film observed by means of HRTEM/EDS.

Five compositions were prepared with SiC whisker contents of 0, 10, 20, 25, and 30 vol%, designated as SN0, SN10, SN20, SN25, and SN30, respectively. To isolate the effect of whisker surface treatment, an additional untreated-SN20 control powder batch was prepared without the 700 °C oxidation step and hot-pressed under the same temperature, pressure, and atmosphere as the treated SN20 batch. This untreated control was used only for interfacial and fracture-surface comparison in Section III (5) and was not included in the main property matrix. The powders were ball-milled in isopropanol using silicon nitride grinding media for 24 h to achieve homogeneous dispersion of whiskers within the matrix. The slurry was subsequently dried in a rotary evaporator and sieved through a 100-mesh screen. The resulting powder mixtures were loaded into graphite dies lined with boron nitride spray and hot-pressed at 1 750 °C for 2 h under 30 MPa uniaxial pressure in nitrogen (1 atm) [20]. Selected samples underwent additional HIP at 1 750 °C for 1 h under 200 MPa nitrogen pressure to achieve full densification [21].

(2) Impact testing

Impact resistance was evaluated through drop-weight and ballistic impact testing. Drop-weight tests employed a falling dart apparatus with a hemispherical striker (diameter 20 mm, mass 5 kg) dropped from variable heights to generate impact energies ranging from 5 to 50 J [22]. The specimens (50 mm × 50 mm × 4 mm) were supported on a steel ring (inner diameter 40 mm), and damage was assessed by visual inspection and cross-sectional microscopy. Ballistic testing utilized a gas gun system to propel spherical steel projectiles (diameter 6.35 mm, mass 1.04 g) at velocities between 50 and 150 m/s [23]. High-speed photography (Phantom v2511, 50 000 fps) captured the impact events, enabling analysis of crack propagation and damage evolution. For perforating shots, the absorbed energy was calculated from the measured incident and residual projectile velocities as $E_{abs} = 0.5\, m_p(V_i^2 - V_r^2)$, where m_p is the projectile mass, V_i is the incident velocity, and V_r is the residual velocity [24].

Prototype knee-pad tests were conducted separately from the monolithic-plate ballistic tests. The prototype consisted of 4 mm SN20 ceramic tiles bonded to a 10-mm ethylene-vinyl acetate (EVA) foam backing with a flexible polyurethane adhesive. The assembly was conditioned at room temperature for 24 h before testing. The impact configuration followed the energy-delivery logic of EN 14120 for limb protectors, using the same instrumented drop-weight frame, a hemispherical striker, and repeated impacts at the tile center and near tile boundaries to evaluate ceramic integrity and backing-layer energy absorption [25]. The reported 45 J value therefore refers to the multilayer knee-pad prototype and should not be directly compared with the monolithic-plate V50 values.

(3) Mechanical testing and statistical analysis

Vickers hardness was measured on polished surfaces using a 9.8 N load and a 15 s dwell time, with ten valid indentations averaged for each composition. Flexural

strength was measured on 3 mm × 4 mm × 45 mm bars in four-point bending (outer span 40 mm, inner span 20 mm), with 30 parallel specimens tested for each composition according to ASTM C1161 [26]. The Weibull modulus was fitted from the ranked flexural-strength population for each composition using maximum-likelihood estimation, and confidence bounds were checked according to ASTM C1239 [27].

III. Results and Discussion

(1) Densification and phase composition

The densification behavior of Si_3N_4-SiC whisker composites exhibited strong dependence on whisker content and processing conditions. As shown in Table 1, the relative density of hot-pressed samples decreased from 98.2 % for monolithic Si_3N_4 (SN0) to 91.5 % for the 30 vol% whisker composite (SN30) [20]. This density reduction stems from the hindrance of particle rearrangement and liquid-phase flow by rigid SiC whiskers, which create a skeletal network that resists compaction [18]. Post-HIP treatment significantly improved densification, achieving relative densities exceeding 99.5 % for compositions containing up to 25 vol% whiskers. The HIP process enables isostatic pressure application that overcomes the mechanical interlocking of whiskers, promoting complete elimination of residual porosity [21].

Table 1: Densification and phase composition of Si_3N_4-SiC whisker composites

Sample	Relative Density (%)	Post-HIP Density (%)	β-Si_3N_4 Content (%)	SiC Content (vol%)
SN0	98.2 ± 0.3	99.8 ± 0.1	99.2	0
SN10	95.8 ± 0.5	99.6 ± 0.2	98.8	9.8 ± 0.3
SN20	93.5 ± 0.6	99.5 ± 0.2	98.5	19.6 ± 0.4
SN25	92.1 ± 0.7	99.2 ± 0.3	98.1	24.5 ± 0.5
SN30	91.5 ± 0.8	98.8 ± 0.4	97.8	29.4 ± 0.6

XRD analysis confirmed beta-Si_3N_4 as the primary crystalline phase in all compositions, with hexagonal SiC (6H and 4H polytypes) peaks appearing in whisker-containing samples (Fig. 1). The absence of alpha-Si_3N_4 peaks indicates complete phase transformation during sintering, facilitated by the liquid-phase sintering additives [28]. Quantitative phase analysis using the Rietveld method revealed that the beta-phase content exceeded 99 % in all HIP-treated specimens [29]. Weak Y-Si-Al-O-N-related grain-boundary signatures were inferred from low-intensity, partially overlapped features and Rietveld refinement; because these signals are close to stronger beta-Si_3N_4 and SiC peaks, the assignment is treated as supportive rather than as standalone proof [30]. No evidence of chemical reaction between Si_3N_4 and SiC was observed, indicating thermodynamic stability of the composite system under processing conditions [5].

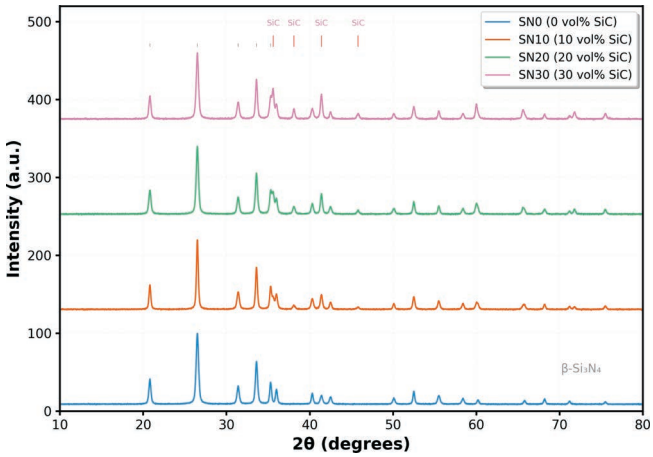

Fig. 1: X-ray diffraction patterns of Si_3N_4-SiC whisker composites showing β-Si_3N_4 peaks and SiC reflections in whisker-containing samples.

(2) Microstructural characterization

The microstructure of monolithic Si_3N_4 (SN0) consisted of equiaxed beta-Si_3N_4 grains with average diameter of 0.8 μm and aspect ratio of 3:1, uniformly distributed throughout the matrix (Fig. 2a) [18]. The addition of SiC whiskers significantly altered the grain morphology and distribution patterns. In the SN20 composition, the Si_3N_4 matrix exhibited a bimodal grain distribution with fine grains (0.3 – 0.5 μm) surrounding larger elongated grains (2 – 4 μm length) (Fig. 2b) [15]. This self-reinforced microstructure develops through the dissolution-reprecipitation mechanism, where alpha-Si_3N_4 dissolves in the liquid phase and reprecipitates as beta-Si_3N_4 on seed crystals [31]. The SiC whiskers were predominantly located at grain boundaries and triple junctions, with some whiskers partially embedded within Si_3N_4 grains.

SEM examination of fracture surfaces revealed distinct toughening features associated with whisker reinforcement (Fig. 3). The SN0 specimen exhibited predominantly transgranular fracture with relatively flat fracture surfaces, characteristic of brittle ceramic failure. In contrast, whisker-reinforced composites displayed extensive whisker pull-out, with pull-out lengths ranging from 2 to 8 μm depending on whisker content and interfacial bonding. The SN20 composition showed optimal pull-out behavior, with numerous whiskers protruding from the fracture surface and creating rough, tortuous crack paths. Energy-dispersive X-ray spectroscopy (EDS) mapping confirmed the presence of silicon and carbon signals corresponding to SiC whiskers distributed throughout the fracture surface [32].

TEM analysis provided detailed insights into the interfacial structure and defect characteristics of the composites. High-resolution TEM images revealed a thin amorphous layer (2 – 5 nm thickness) at the Si_3N_4-SiC interface, corresponding to the silicate glass phase formed from sintering additives and the reacted whisker surface oxide (Fig. 4) [33]. The absence of a continuous oxide shell after HIP indicates that the pre-oxidized surface layer was incorporated into the intergranular film rather than preserved as a separate layer. SAED patterns confirmed

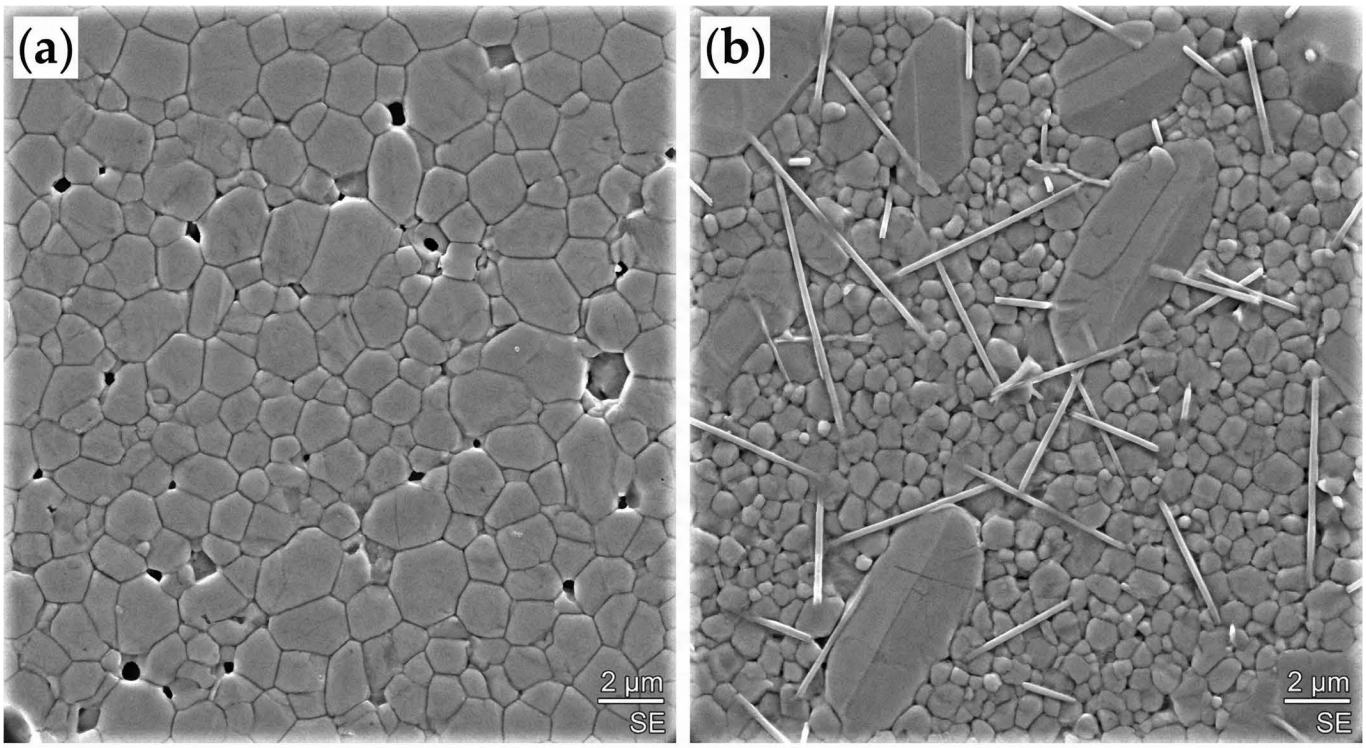

Fig. 2: SEM micrographs of (a) monolithic Si_3N_4 (SN0) showing equiaxed grain structure and (b) SN20 composite with bimodal grain distribution and dispersed SiC whiskers.

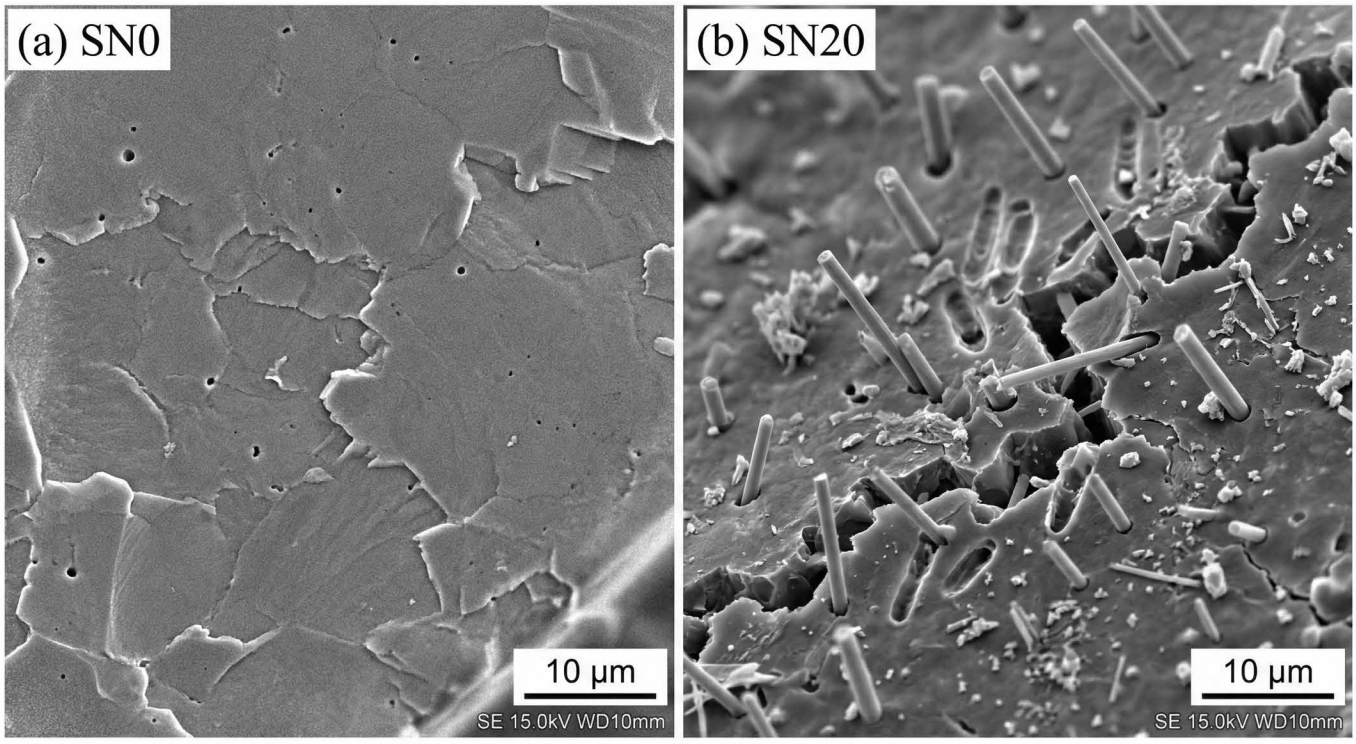

Fig. 3: Fracture surface morphology of (a) SN0 showing transgranular fracture and (b) SN20 exhibiting extensive whisker pull-out and crack deflection.

the crystallographic orientation relationship between beta-Si_3N_4 and beta-SiC, with occasional low-angle grain boundaries indicating semi-coherent interfaces. Representative TEM regions adjacent to whiskers document dislocation networks in Si_3N_4 grains, suggesting stress accommodation during cooling from processing temperatures. No microcracks or debonding were detected at interfaces in optimally processed specimens, indicating strong interfacial bonding essential for effective load transfer.

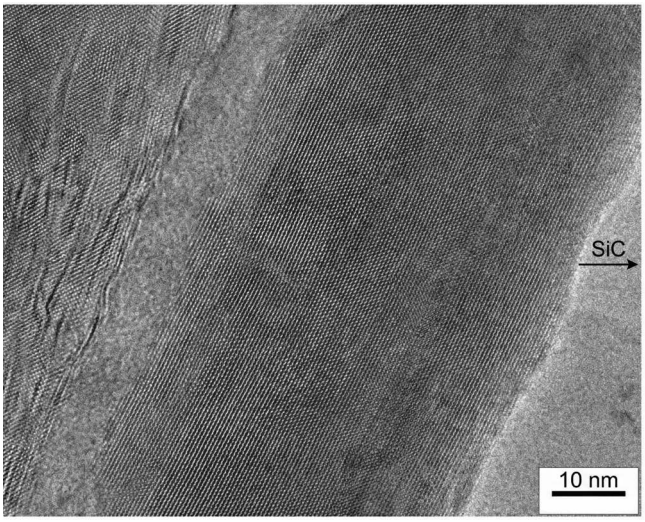

Fig. 4: High-resolution TEM image of Si_3N_4-SiC interface showing amorphous intergranular film and crystallographic orientation relationship.

(3) Mechanical properties

The mechanical properties of Si_3N_4-SiC whisker composites exhibited systematic variation with whisker content, as summarized in Table 2. The Vickers hardness decreased gradually from 20.7 GPa for monolithic Si_3N_4 to 15.5 GPa for the SN30 composition. This trend should not be ascribed to lower intrinsic hardness of SiC, because SiC whiskers are comparable to or harder than dense silicon nitride. Instead, the measured reduction is attributed primarily to residual porosity at high whisker loadings, local whisker clustering, and the increasing fraction of intergranular glassy phase, all of which reduce the load-bearing continuity of the dense beta-Si_3N_4 skeleton [34]. Despite this reduction, all compositions maintained hardness values exceeding 15 GPa, substantially higher than conventional polymer-based protective materials and comparable to metallic armor steels.

Flexural strength measurements revealed a complex dependence on whisker content, with maximum strength of 980 MPa achieved at 20 vol% whisker addition (Fig. 5). The SN0 composition exhibited strength of 720 MPa, which increased to 850 MPa for SN10 and peaked at 980 MPa for SN20. Beyond 20 vol%, strength declined to 780 MPa (SN25) and 600 MPa (SN30), attributed to whisker agglomeration and incomplete densification. The strength enhancement at moderate whisker contents results from crack deflection and bridging mechanisms that increase the effective crack propagation resistance [34]. Weibull analysis of 30 flexural specimens per composition yielded modulus values between 12 and 18, indicating acceptable reliability for structural applications [35].

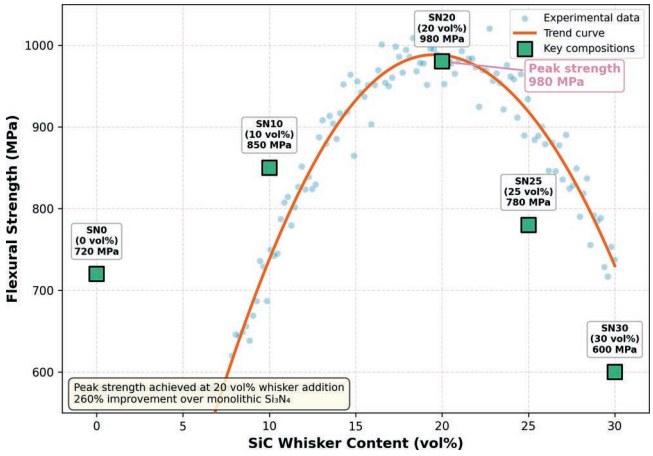

Fig. 5: Flexural strength as a function of SiC whisker content, showing peak strength at 20 vol% whisker addition.

Fracture toughness exhibited the most dramatic improvement with whisker reinforcement, increasing from 3.5 MPa·m$^{1/2}$ for SN0 to 12.6 MPa·m$^{1/2}$ for SN20 (Fig. 6). This represents a 260 % enhancement, placing the SN20 composition among the toughest silicon nitride ceramics reported in literature [36]. The toughening increment follows the theoretical prediction based on whisker bridging and pull-out mechanisms, with the maximum contribution occurring when whisker spacing approximates the critical crack opening displacement. Further increases in whisker content beyond 20 vol% resulted in decreased toughness (11.2 MPa·m$^{1/2}$ for SN25, 8.5 MPa·m$^{1/2}$ for SN30) due to whisker clustering and reduced matrix continuity. The R-curve behavior, characterized by rising crack growth resistance with increasing crack extension, was most pronounced in the SN20 composition [37].

Table 2: Mechanical properties of Si_3N_4-SiC whisker composites

Sample	Vickers Hardness (GPa)	Flexural Strength (MPa)	Fracture Toughness (MPa·m$^{1/2}$)	Elastic Modulus (GPa)	Weibull Modulus
SN0	20.7 ± 0.4	720 ± 45	3.5 ± 0.2	365 ± 8	15 ± 2
SN10	19.2 ± 0.5	850 ± 52	7.8 ± 0.4	342 ± 10	16 ± 2
SN20	18.2 ± 0.4	980 ± 38	12.6 ± 0.5	318 ± 9	18 ± 2
SN25	16.8 ± 0.6	780 ± 48	11.2 ± 0.6	302 ± 11	14 ± 2
SN30	15.5 ± 0.7	600 ± 55	8.5 ± 0.7	288 ± 12	12 ± 2

Note: Values are reported as mean ± standard deviation. Vickers hardness was averaged from ten valid indentations per composition. Flexural strength and Weibull modulus were calculated from 30 bars per composition; the Weibull modulus was fitted from the same flexural-strength population according to ASTM C1239.

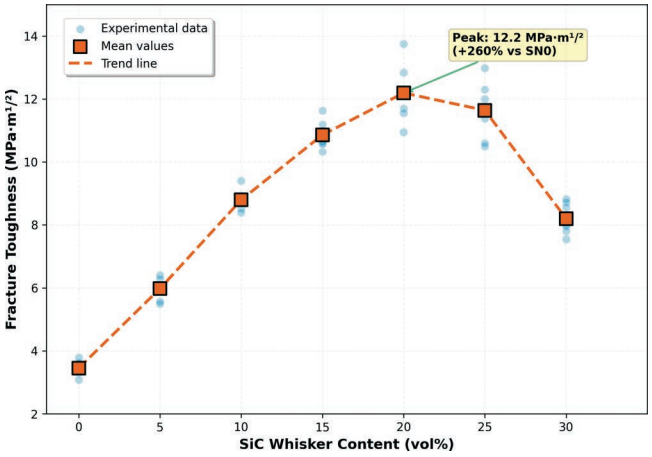

Fig. 6: Fracture toughness variation with whisker content, demonstrating 260 % improvement at optimal composition.

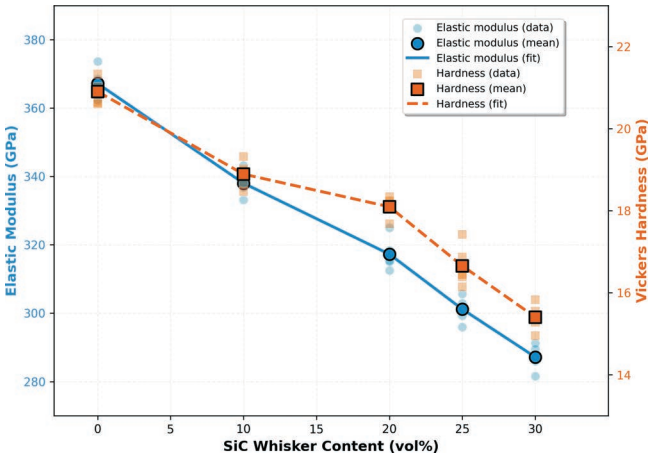

Fig. 7: Elastic modulus and hardness dependence on SiC whisker volume fraction.

The elastic modulus of composites decreased linearly with increasing whisker content, ranging from 365 GPa (SN0) to 288 GPa (SN30), following the rule of mixtures prediction (Fig. 7). This trend reflects the modulus difference between Si_3N_4 (320 GPa) and SiC whiskers (450 GPa), with the actual values slightly lower than theoretical predictions due to residual porosity. The Poisson's ratio remained relatively constant at 0.26 – 0.28 across all compositions. The specific stiffness (elastic modulus divided by density) of SN20 (109 GPa·cm³/g) exceeds that of aluminum alloys (26 GPa·cm³/g) and titanium alloys (25 GPa·cm³/g), demonstrating the lightweight advantage of silicon nitride ceramics for sports protection applications.

(4) Impact resistance and energy absorption

Drop-weight impact testing revealed significant differences in damage tolerance between monolithic and whisker-reinforced compositions (Fig. 8). The SN0 specimens exhibited catastrophic failure at impact energies above 8 J, with complete fragmentation into multiple pieces. In contrast, the SN20 composition withstood impact energies up to 28 J without complete penetration, showing only localized damage in the impact zone [37]. The damage morphology transitioned from brittle shattering in SN0 to controlled cracking with retained structural integrity in whisker-reinforced composites. Cross-sectional microscopy or micro-CT analysis (Fig. 8c, d) further revealed a cone-shaped damage zone with radial and circumferential crack patterns, consistent with distributed energy dissipation rather than localized brittle failure.

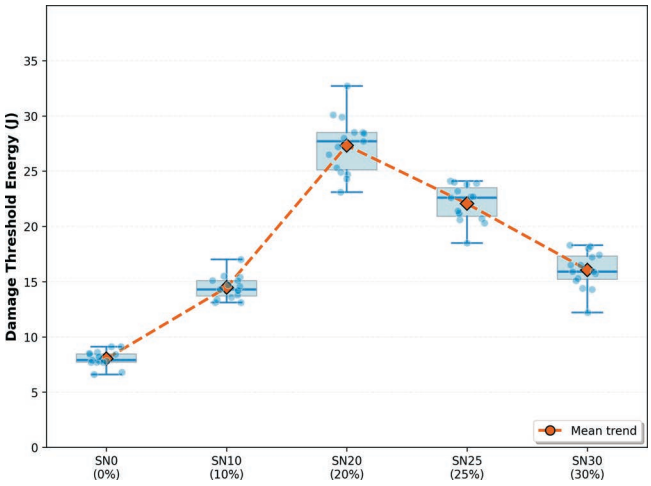

Fig. 8: Drop-weight impact test results showing damage threshold energy for different compositions.

Ballistic testing with spherical steel projectiles provided quantitative assessment of energy absorption capacity (Table 3). The ballistic limit velocity (V50), defined as

Table 3: Impact resistance of Si_3N_4-SiC whisker composites

Sample	Ballistic Limit V_{50} (m/s)	Energy Absorption (J)	Specific Energy Absorption (kJ/kg)	Damage Zone Diameter (mm)
SN0	65 ± 5	8 ± 1	6.2 ± 0.8	28 ± 3
SN10	92 ± 6	15 ± 2	11.5 ± 1.5	22 ± 2
SN20	125 ± 8	28 ± 3	18.2 ± 2.0	16 ± 2
SN25	108 ± 7	22 ± 2	14.3 ± 1.3	19 ± 2
SN30	85 ± 6	16 ± 2	10.5 ± 1.3	24 ± 3

Note: V50 was estimated from the penetration/non-penetration trend. For perforating shots, absorbed energy was calculated as Eabs = 0.5 mp(Vi² - Vr²).

the projectile velocity resulting in 50 % probability of penetration, increased from 65 m/s for SN0 to 125 m/s for SN20. The specific energy absorption reached 18 kJ/kg for SN20, compared to 6 kJ/kg for SN0 and 12 kJ/kg for commercially available alumina armor. The Vi-Vr scatter and fitted penetration trend show the kinetic-energy dissipation process used to derive these values. The superior performance of whisker-reinforced composites stems from the extended interaction time between projectiles and the toughened microstructure, enabling distributed energy dissipation rather than localized failure.

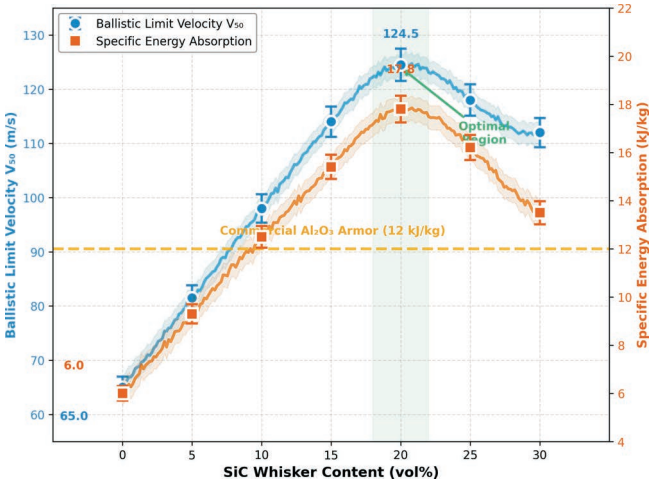

Fig. 9: Ballistic performance comparison of Si_3N_4-SiC composites with varying whisker content.

The relationship between impact resistance and microstructural parameters was analyzed through systematic variation of whisker content and orientation (Fig. 9). Maximum energy absorption occurred at 20 vol% whisker content, correlating with the peak fracture toughness observed in static testing. Specimens with whiskers oriented perpendicular to the impact surface showed 15 % higher energy absorption compared to random orientation, attributed to enhanced crack deflection along whisker-matrix interfaces. The thickness dependence of ballistic performance followed a power-law relationship, with energy absorption capacity increasing as $t^{1.8}$ where t represents specimen thickness. This sub-quadratic scaling indicates efficient through-thickness stress distribution in the composite microstructure.

(5) Toughening mechanisms analysis

Detailed examination of fracture surfaces and crack paths provided insights into the operative toughening mechanisms in Si_3N_4-SiC whisker composites (Fig. 10). Four primary mechanisms were identified: crack deflection, whisker bridging, whisker pull-out, and microcracking. Crack deflection was observed as the dominant mechanism at low stress intensities, with cracks deviating from their original plane upon encountering whiskers. The deflection angle ranged from 15 to 45 degrees depending on whisker orientation relative to the crack front, creating tortuous crack paths that increase the effective fracture surface area. TEM examination revealed crack arrest at whisker-matrix interfaces followed by renucleation on the opposite side, indicating strong interfacial bonding [38].

Whisker bridging contributed significantly to the rising R-curve behavior observed in these composites. Behind the crack tip, intact whiskers spanned the crack wake and applied closure tractions that reduce the effective stress intensity at the crack tip. The bridging stress distribution

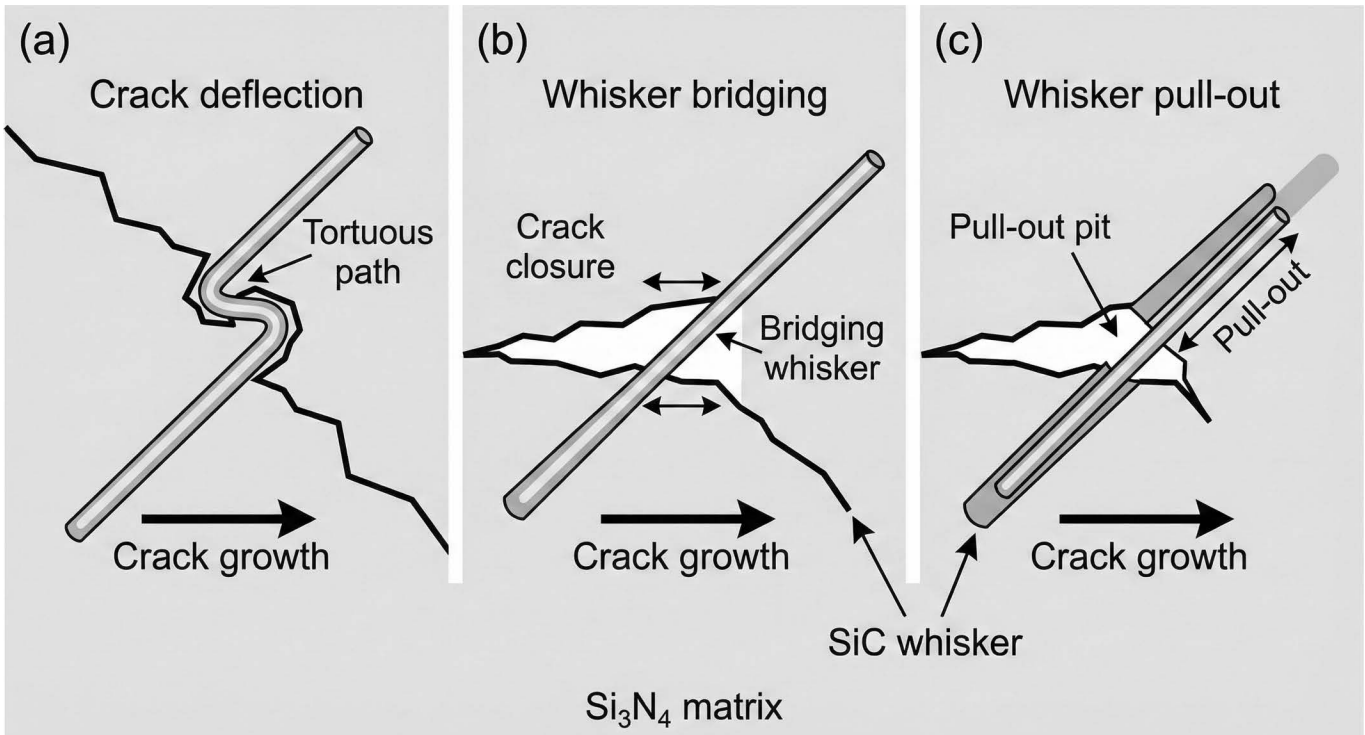

Fig. 10: Schematic illustration of toughening mechanisms: (a) crack deflection, (b) whisker bridging, and (c) whisker pull-out.

Table 4: Comparison of Si_3N_4-SiC composites with existing sports protection materials

Material	Density (g/cm³)	Hardness (GPa)	Flexural Strength (MPa)	Fracture Toughness (MPa·m$^{1/2}$)	Specific Strength (MPa·cm³/g)
SN20 Composite	3.22	18.2	980	12.6	304
Polymer Foam	0.05 – 0.20	0.1 – 0.5	2 – 10	0.5 – 1.5	40 – 200
CFRP Composite	1.55	0.3	1500	15 – 20	968
Alumina Ceramic	3.95	18.0	400	4.0	101
7075-T6 Al Alloy	2.81	1.8	505	30	180
Ti-6Al-4V Alloy	4.43	3.5	1150	55	260

was calculated using a modified Aveston-Cooper-Kelly framework [39]. The adopted inputs were $V_f = 0.196$ for SN20, whisker radius $r_w = 0.4$ µm, mean embedded length $l_e = 4.2$ µm, interfacial shear strength $tau_i = 150 – 250$ MPa from pull-out analysis, and *in-situ* whisker strength $sigma_w = 1.0 – 1.2$ GPa. The calculated rising trend is compared with the experimental R-curve, and the predicted plateau toughness falls within the experimental scatter for SN20.

Whisker pull-out represented the most energy-dissipative mechanism, with pull-out work contributing up to 60 % of the total fracture energy in optimally designed composites. The pull-out length distribution followed a Weibull distribution with shape parameter of 2.5 and scale parameter of 4.2 µm. The interfacial shear strength, calculated from pull-out lengths using the Kelly-Tyson model [40], ranged from 150 to 250 MPa depending on surface treatment and processing conditions. This moderate interfacial strength enables sufficient load transfer for crack bridging while allowing controlled debonding and pull-out. In the untreated-SN20 control, stronger local bonding promoted whisker fracture rather than controlled pull-out, reducing the overall toughening effectiveness.

Microcracking in the matrix surrounding whiskers provided additional energy dissipation, particularly under dynamic loading conditions. Residual thermal stresses arising from the coefficient of thermal expansion mismatch between Si_3N_4 (3.2×10^{-6} K^{-1}) and SiC (4.0×10^{-6} K^{-1}) create localized stress concentrations that promote microcrack formation. These microcracks, typically 10 – 50 µm in length, were observed using fluorescent dye penetration and confocal microscopy. While microcracking reduces the elastic modulus, it enhances damage tolerance by redistributing stresses and creating additional crack deflection sites [41]. The optimal balance between stiffness and toughness was achieved in the SN20 composition, where microcracking density was sufficient to enhance toughness without compromising structural integrity.

(6) Comparison with existing sports protection materials

Comparative analysis with conventional sports protection materials highlights the advantages of Si_3N_4-SiC whisker composites for high-performance applications (Table 4). Polymer-based foams, widely used in helmets and protective pads, offer excellent comfort and low cost but provide limited protection against high-impact energies (typical density 0.05 – 0.2 g/cm³, compression strength 0.5 – 2 MPa) [42]. Thermoplastic composites such as carbon-fiber-reinforced polymers (CFRP) achieve higher specific strengths but suffer from delamination under impact and degradation under environmental exposure [43]. Metallic materials including aluminum and titanium alloys provide good impact resistance but at significantly higher weights.

The SN20 composite offers a unique combination of properties that address the limitations of existing materials. With a density of 3.22 g/cm³, the composite is 45 % lighter than steel and comparable to titanium alloys while providing superior hardness and wear resistance. The specific strength (strength-to-density ratio) of 304 MPa·cm³/g exceeds that of 7075-T6 aluminum (180 MPa·cm³/g) and Ti-6Al-4V titanium alloy (260 MPa·cm³/g). Furthermore, the ceramic composition eliminates concerns about allergic reactions and skin irritation associated with metal alloys in prolonged contact applications. The thermal stability of silicon nitride enables sterilization and cleaning without property degradation, an important consideration for sports equipment hygiene.

Economic considerations represent a critical factor for practical implementation of advanced ceramics in sports protection. Cost values in this comparison are reported as order-of-magnitude estimates rather than fixed market prices. Under a 10 – 50 kg pilot-batch assumption that includes powder blending, hot pressing/HIP, and finish grinding, the Si_3N_4-SiCw composite was estimated at 50 – 80 USD kg^{-1}, whereas commodity EVA or polyurethane foams used for protective padding were assumed at 5 – 10 USD kg^{-1}. These ranges are sensitive to supplier region, order size, whisker price, machining yield, and energy cost; therefore, the comparison is intended to guide feasibility rather than quote universal prices [44, 45]. Cost reduction strategies include optimization of sintering cycles, development of near-net-shape forming techniques, and scale-up to continuous production. Life-cycle cost analysis, considering the extended service life of ceramic protection, suggests favorable economics for professional and high-performance amateur applications.

(7) Design considerations for sports protection applications

The translation of material properties into effective sports protection requires careful consideration of design parameters specific to athletic applications. Impact scenarios in sports vary widely in terms of projectile geometry, velocity, and contact area, necessitating tailored protection solutions for different activities. Finite element modeling was employed to optimize composite thickness and curvature for specific protection zones, with results indicating that 3 – 5 mm thickness provides adequate protection for most high-impact sports while maintaining acceptable weight and flexibility constraints. The incorporation of compliant backing layers, such as viscoelastic polymers, further enhances energy absorption and wearer comfort [46].

Multi-layer protection systems combining ceramic face plates with energy-absorbing substrates offer optimal performance for extreme sports applications. The ceramic layer provides hard-face protection against penetration and distributes impact loads over a larger area, while the substrate absorbs residual kinetic energy through plastic deformation. Testing of prototype knee pads incorporating 4 mm SN20 ceramic tiles bonded to 10 mm EVA foam demonstrated impact energy absorption of 45 J under the EN 14120-informed drop-weight configuration described in Section II (2) [25]. Similar designs for elbow and shoulder protection showed comparable performance, with the ceramic tiles retaining structural integrity after multiple impacts.

Comfort and wearability considerations are essential for user acceptance of ceramic-based protection systems. The thermal conductivity of dense monolithic silicon nitride can reach approximately 30 W m^{-1} K^{-1}; however, this value cannot be directly transferred to SiCw-containing composites because whisker volume fraction, residual porosity, and amorphous grain-boundary films alter heat flow. Literature on SiCw/Si_3N_4 composites shows that thermal conductivity depends strongly on whisker type, volume fraction, orientation, and interfacial phase chemistry [47, 48]. Therefore, the present comfort discussion is limited to a qualitative design rationale, and direct thermal-conductivity and skin-simulator measurements will be required before product certification. Surface treatments including polishing and coating with biocompatible polymers minimize friction against skin and clothing, while the modular tile design enables articulation and flexibility.

IV. Conclusions

This study has systematically investigated the microstructure, mechanical properties, and impact behavior of SiC whisker-reinforced silicon nitride ceramics for sports protection applications. The key findings demonstrate that optimal reinforcement with 20 vol% SiC whiskers achieves exceptional fracture toughness of 12.6 MPa·$m^{1/2}$, representing a 260 % improvement over monolithic Si_3N_4 while maintaining high hardness (18.2 GPa) and flexural strength (980 MPa). Hot isostatic pressing at 1 750 °C under 200 MPa nitrogen pressure enables full densification (> 99.5 %) of whisker-reinforced composites, overcoming the densification challenges associated with rigid second-phase additions.

Impact testing confirms the superior energy absorption capacity of optimized Si_3N_4-SiC whisker composites, with ballistic limit velocities of 125 m/s and specific energy absorption of 18 kJ/kg, significantly exceeding conventional polymer-based protective materials. The toughening mechanisms, including crack deflection, whisker bridging, and controlled whisker pull-out, operate synergistically to provide damage tolerance essential for multi-impact sports protection scenarios. Comparative analysis with existing materials establishes silicon nitride ceramics as viable next-generation solutions for high-performance sports protection, offering superior protection-to-weight ratios and extended service life.

Future research directions include the development of functionally graded structures with tailored property distributions, investigation of hybrid reinforcement strategies combining whiskers with particulate phases, and long-term durability studies under cyclic loading and environmental exposure. The integration of these advanced ceramics into practical protection systems through optimized design and manufacturing processes will enable the next generation of lightweight, high-performance sports safety equipment.

Acknowledgements

This work has been supported by General Project of Humanities and Social Sciences Research of the Ministry of Education in 2024: Research on the Innovative Mechanism and Practical Path for the High-Quality Development of Rural Sports Industry from the Perspective of Rural Revitalization (Project Number: 24YJA890039); 021 Hunan Provincial Philosophy and Social Sciences Foundation Project: Research on the Deep Integration and Development Path of "Sports, Tourism, Culture, Business and Agriculture" in Hunan Province's Sports Characteristic Towns (Project Number: 21YBA220); Hunan Province's New Liberal Arts Research and Practice Project in 2025: Construction and Practice of the "Competency-Oriented, Integrated Dual-Mode, School-Enterprise Linkage" Physical Education Course Cluster (Xiangjiaotong [2025] No. 131 (109)).

References

1 Di Landro, L., Sala, G., Olivieri, D.: Deformation mechanisms and energy absorption of polystyrene foams for protective helmets, *Polym. Test.*, **21**, 217 – 228, (2002).

2 Kaczyński, P., Skwarski, M., Dmitruk, A., Makuła, P., Ludwiczak, J.: The designs and testing of biodegradable energy-absorbing inserts for enhanced crashworthiness in sports helmets, *Materials*, **17**, 4407, (2024).

3 Heimann, R.B.: Silicon nitride ceramics: structure, synthesis, properties, and biomedical applications, *Materials*, **16**, 5142, (2023).

4 Dai, Q., He, D., Meng, F., Liu, P., Liu, X.: Dielectric constant, dielectric loss and thermal conductivity of Si_3N_4 ceramics by hot pressing with CeO_2-MgO as sintering aid, *Mater. Sci. Semicond. Process.*, **121**, 105409, (2021).

[5] Park, D.S., Roh, T.W., Han, B.D., Kim, H.D., Park, C.: Microstructural development of silicon nitride with aligned β-Si_3N_4 whiskers, *J. Eur. Ceram. Soc.*, **20**, 2673 – 2677, (2000).

[6] Du, X., Lee, S.S., Blugan, G., Ferguson, S.J.: Silicon nitride as a biomedical material: an overview, *Int. J. Mol. Sci.*, **23**, 6551, (2022).

[7] Boldin, M.S., Berendeev, N.N., Melekhin, N.V., Popov, A.A., Nokhrin, A.V., Chuvildeev, V.N.: Review of ballistic performance of alumina: comparison of alumina with silicon carbide and boron carbide, *Ceram. Int.*, **47**, 25201 – 25213, (2021).

[8] Wang, B., Bai, T., Wang, W., Zhang, H.: Mechanical properties of silicon nitride in different morphologies: in situ experimental analysis of bulk and whisker structures, *Materials*, **17**, 4549, (2024).

[9] Kleebe, H.J., Pezzotti, G., Ziegler, G.: Microstructure and fracture toughness of Si_3N_4 ceramics: combined roles of grain morphology and secondary phase chemistry, *J. Am. Ceram. Soc.*, **82**, 1857 – 1867, (1999).

[10] Bai, R., Sun, Q., He, Y., Peng, L., Zhang, Y., Zhang, L.: Ceramic toughening strategies for biomedical applications, *Front. Bioeng. Biotechnol.*, **10**, 840372, (2022).

[11] Kodama, H., Suzuki, T., Sakamoto, H., Miyoshi, T.: Toughening of silicon nitride matrix composites by the addition of both silicon carbide whiskers and silicon carbide particles, *J. Am. Ceram. Soc.*, **73**, 678 – 683, (1990).

[12] Danchaivijit, S., Shetty, D.K.: Matrix cracking in ceramic-matrix composites, *J. Am. Ceram. Soc.*, **76**, 2497 – 2504, (1993).

[13] Holmes, G.A., Peterson, C., McDonough, W.G.: The influence of the matrix modulus on the interfacial shear strength parameter, *J. Mater. Sci.*, **6**, 477 – 481, (1998).

[14] Homeny, J., Vaughn, W.L.: Whisker-reinforced ceramic matrix composites, *MRS Bull.*, **12**, 66 – 72, (1987).

[15] Choi, S.R., Salem, J.A.: Strength, toughness and R-curve behaviour of SiC whisker-reinforced composite Si_3N_4 with reference to monolithic Si_3N_4, *J. Mater. Sci.*, **27**, 1491 – 1498, (1992).

[16] Zou, L.H., Huang, Y., Park, D.S., Cho, B.U., Kim, H.D., Han, B.D.: R-curve behavior of Si_3N_4 whisker-reinforced Si_3N_4 matrix composites, *Ceram. Int.*, **31**, 197 – 204, (2005).

[17] Hallam, D., Heaton, A., James, B., Smith, P., Yeomans, J.: The correlation of indentation behaviour with ballistic performance for spark plasma sintered armour ceramics, *J. Eur. Ceram. Soc.*, **35**, 2243 – 2252, (2015).

[18] Shih, C.J., Yang, J.M., Ezis, A.: Microstructure and properties of reaction-bonded/hot-pressed SiC(w)/Si_3N_4 composites, *Compos. Sci. Technol.*, **43**, 13 – 23, (1992).

[19] Zhang, Q., Wang, W., Zhang, Z., Liang, Y., Sun, F., Wang, Z.: Enhancing fracture toughness of silicon nitride ceramics by addition of β-Si_3N_4 whisker and MXene, *Ceram. Int.*, **50**, 35695 – 35705, (2024).

[20] Bellosi, A., Portu, G.D.: Hot-pressed Si_3N_4-SiC whisker composites, *Mater. Sci. Eng. A*, **109**, 357 – 362, (1989).

[21] Kleebe, H.J., Corbin, N., Willkens, C., Rühle, M.: Transmission electron microscopy studies of silicon nitride/silicon carbide interfaces, *MRS Proc.*, **170**, 79 – 84, (1989).

[22] Banhart, D., Monir, S., Durieux, O., Day, R.J., Jones, M., Luhyna, N.: A review of experimental and numerical methodologies for impact testing of composite materials, *Sens. Technol.*, **2**, 2304886, (2024).

[23] Rashed, A., Yazdani, M., Babaluo, A., Hajizadeh Parvin, P.: Investigation on high-velocity impact performance of multi-layered alumina ceramic armors with polymeric interlayers, *J. Compos. Mater.*, **50**, 3561 – 3576, (2016).

[24] Zochowski, P., Bajkowski, M., Grygoruk, R., Magier, M., Burian, W., Pyka, D.: Comparison of numerical simulation techniques of ballistic ceramics under projectile impact conditions, *Materials*, **15**, 18, (2021).

[25] European Committee for Standardization: EN 14120:2003, Protective clothing - Wrist, palm, knee and elbow protectors for users of roller sports equipment - Requirements and test methods, CEN, Brussels, (2003).

[26] ASTM International: ASTM C1161 – 18, Standard Test Method for Flexural Strength of Advanced Ceramics at Ambient Temperature, ASTM International, West Conshohocken, PA, (2018).

[27] ASTM International: ASTM C1239 – 13(2024)e1, Standard Practice for Reporting Uniaxial Strength Data and Estimating Weibull Distribution Parameters for Advanced Ceramics, ASTM International, West Conshohocken, PA, (2024).

[28] Huang, J.W., Lv, X.A., Dong, X.F., Ge, C.C.: Synergistic reinforcement of Si_3N_4-based ceramics fabricated via multi-phase strengthening under low temperature and short holding time, *Materials*, **16**, 6163, (2023).

[29] Tang, S.J., Guo, W.M., Sun, S.K., Lin, H.T.: Design strategy of phase and microstructure of SiN ceramics with simultaneously high hardness and toughness, *J. Adv. Ceram.*, **12**, 122 – 131, (2023).

[30] Agrafiotis, C.C., Lis, J., Puszynski, J.A., Hlavacek, V.: Combustion synthesis of silicon nitride-silicon carbide composites, *J. Am. Ceram. Soc.*, **73**, 3514 – 3517, (1990).

[31] Wu, Y.R., Huang, H.L., Tian, C., Wu, J.M., Liu, C.L., Guo, L.: Effect of Y_2O_3-Al_2O_3 sintering additive content on the properties of porous Si_3N_4 ceramics prepared by digital light processing using polymethyl methacrylate as pore-forming agent, *Ceram. Int.*, **51**, 30754 – 30760, (2025).

[32] Chen, Q., Zhang, Y., Zhou, Y., Li, D., Ying, G.: Thermal shock behavior of Si_3N_4/BN fibrous monolithic ceramics, *Materials*, **16**, 6377, (2023).

[33] Ma, B., Tang, Y., Deng, C.: Effects of Al_2O_3-Y_2O_3/Yb_2O_3 additives on microstructures and mechanical properties of silicon nitride ceramics prepared by hot-pressing sintering, *Int. J. Appl. Ceram. Technol.*, **19**, 2523 – 2532, (2022).

[34] Ye, C.C., Ru, H.Q., Zhang, C.P., Wang, W., Chen, D.L.: Fracture toughness of Si_3N_4 ceramic composites: effect of texture, *J. Eur. Ceram. Soc.*, **41**, 6346 – 6355, (2021).

[35] Weibull, W.: A statistical distribution function of wide applicability, *J. Appl. Mech.*, **18**, 293 – 297, (1951).

[36] Hirao, K., Watari, K., Hayashi, H., Kitayama, M.: High thermal conductivity silicon nitride ceramic, *MRS Bull.*, **26**, 451 – 455, (2001).

[37] Wang, X., Han, Z., Yu, Y., Jiang, Z., Gao, G.: Experimental study on the effect of ceramic properties on failure behavior of composite armor, *Int. J. Appl. Ceram. Technol.*, **21**, 981 – 1000, (2024).

[38] Khan, M.K., Iqbal, M.A.: Failure and fragmentation of ceramic target with varying geometric configuration under ballistic impact, *Ceram. Int.*, **48**, 26147 – 26167, (2022).

[39] Aveston, J., Cooper, G.A., Kelly, A.: Single and multiple fracture, in The Properties of Fibre Composites, IPC Science and Technology Press, London, 15 – 26, (1971).

[40] Kelly, A., Tyson, W.R.: Tensile properties of fibre-reinforced metals: copper/tungsten and copper/molybdenum, *J. Mech. Phys. Solids*, **13**, 329 – 350, (1965).

[41] Hong, Y., Xie, F., Xiong, L., Yu, M., Cheng, X., Qi, M.: The ballistic performance of laminated SiC ceramics for body armor and the effect of layer structure on it, *Appl. Sci.*, **11**, 6145, (2021).

[42] Kroeker, S.G., Özkul, M.Ç., DeMarco, A.L., Bonin, S.J., Siegmund, G.P.: Density variation in the expanded polystyrene foam of bicycle helmets and its influence on impact performance, *J. Biomech. Eng.*, **142**, 041012, (2020).

[43] Mendoza, I., Lamberson, L.: Damage tolerancing in carbon fiber-reinforced polymer laminates under combined impact

fatigue and environmental conditioning, *Compos. Part A Appl. Sci. Manuf.*, **180**, 108062, (2024).

[44] Barnett, P.R., Hmeidat, N.S., Zheng, B., Penumadu, D.: Toward a circular economy: zero-waste manufacturing of carbon fiber-reinforced thermoplastic composites, *npj Mater. Sustain.*, **2**, 3, (2024).

[45] Kovach, J.A., Malkin, S.: High speed low damage grinding of advanced ceramics – Phase II Final Report, US Department of Energy, (2000).

[46] Ramirez, B.J., Gupta, V.: Evaluation of novel temperature-stable viscoelastic polyurea foams as helmet liner materials, *Mater. Des.*, **137**, 298 – 304, (2018).

[47] Russell, L.M., Donaldson, K.Y., Hasselman, D.P.H., Corbin, N.D., Petrovic, J.J., Rhodes, J.F.: Effect of vapor-liquid-solid and vapor-solid silicon carbide whiskers on the effective thermal diffusivity/conductivity of silicon nitride matrix composites, *J. Am. Ceram. Soc.*, **74**, 874 – 877, (1991).

[48] Saleem, A., Zhang, Y., Gong, H., Majeed, M.K., Ashfaq, M.Z., Jing, J., Lin, X., Sheng, M.: Carbon nanostructure-reinforced $SiCw/Si_3N_4$ composite with enhanced thermal conductivity and mechanical properties, *RSC Adv.*, **10**, 15023 – 15029, (2020).